

Molecular Dynamics Simulations of Surfactant Functionalized Nanoparticles in the Vicinity of an Oil/Water Interface

R. J. K. Udayana Ranatunga, Robert J. B. Kalesky, Chi-cheng Chiu, and Steven O. Nielsen*

Department of Chemistry, University of Texas at Dallas, 800 West Campbell Road, Richardson, Texas 75080

Received: June 10, 2010

The localization of nanoparticles (NPs) at fluid/fluid interfaces has emerged as an effective self-assembly method. To understand the fundamentals of this localization mechanism, it is necessary to quantify the physical behavior of NPs in the vicinity of a fluid interface. Conventional theories treat the NP as a rigid object whose equilibrium position is dictated by the balance of its surface tensions with the two fluids. However, most NPs are functionalized with “soft” organic surface layers which play a large role in determining the shape of the NP. Through molecular dynamics simulations, we show that the functionalizing layer also greatly alters the interfacial behavior of the NP beyond the scope of common theory. Furthermore, we characterize the effect of the surface density of functionalizing molecules on the NP deformability. Our results have implications on the experimental interpretation of NP contact angles and may be useful for future theory development.

Introduction

Scientific advances in recent decades have uncovered the unique properties of nanoparticles (NPs) and the wide array of materials that may be used to create them.^{1,2} In many cases the success of incorporating NPs into industrial applications relies on the ability to control their spatial arrangement.^{2–4} In this respect the self-assembly of NPs at a fluid/fluid interface is an elegant organizational method which allows some control over the geometry of the NP superstructure.^{4,5} For example, Langmuir trough techniques allow mechanical tuning of the interparticle spacing in these two-dimensional assemblies,⁶ as well as their deposition onto solid supports.⁷

The study of NPs at interfaces can be decomposed into the energetics of localization at the interface, and the interparticle interactions which arise among localized NPs. In this study we focus on the affinity of individual NPs to adsorb at the interface of two immiscible bulk phases, specifically at the interface between oil and water. A simple treatment of the energetics of particles at fluid/fluid interfaces was proposed by Pieranski, who reformulated Young’s 1805 force balance argument from an interfacial free energy viewpoint.⁸ According to this theory, for a spherical particle (p) the free energy change as a function of the particle position (η shown in Figure 1) can be given as

$$\Delta G(\eta) = 2\pi R^2(1 + \eta/R)(\gamma_{pw} - \gamma_{po}) - \gamma_{ow}\pi(R^2 - \eta^2) \quad (1)$$

$$-R < \eta < R$$

where ΔG is the free energy measured relative to the particle being completely immersed in oil ($\eta = -R$), R is the radius of the particle, and γ_{pw} , γ_{po} , and γ_{ow} are the particle/water, particle/oil, and oil/water surface tensions, respectively.

Equation 1 suggests that the driving force for adsorption of the particle at an oil/water interface is the removal of unfavorable contact between the two liquids. For a particle of radius R , the

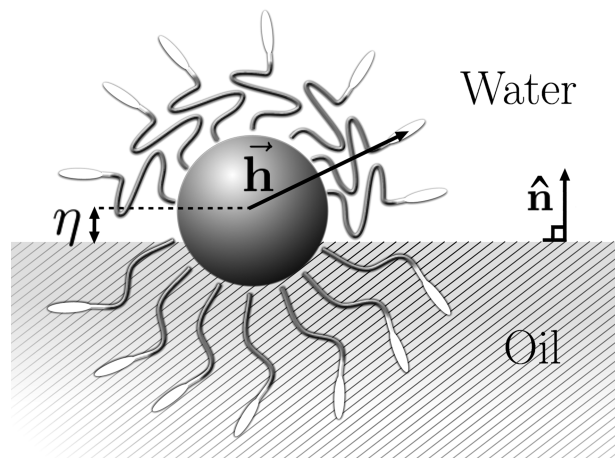


Figure 1. Schematic of a surfactant functionalized NP in the vicinity of a fluid–fluid interface. The core is displaced from the interface by η . \mathbf{h} is the NP center to ligand head vector while $\hat{\mathbf{n}}$ denotes the unit vector normal to the interface. For our studies the surfactant ligand is di(ethylene glycol) dodecyl ether, $\text{CH}_3-(\text{CH}_2)_{11}-(\text{OC}_2\text{H}_4\text{O})_2-\text{H}$.⁹

oil to water transfer free energy is given by $\Delta G_{o \rightarrow w} = 4\pi R^2(\gamma_{pw} - \gamma_{po})$ and the equilibrium position of the particle, η_0 , can be extracted from the minimum value of eq 1, giving the well-known Young’s equation

$$\cos(\theta_0) = \eta_0/R = (\gamma_{po} - \gamma_{pw})/\gamma_{ow} \quad (2)$$

In recent years treatments of rigid nanoscale particles at fluid interfaces have incorporated concepts such as line tension,^{10,11} the Tolman length,¹² and capillary wave broadening¹³ to supplement Young’s theory. In essence these treatments involve lower order terms in R which are neglected by Young’s theory but grow in significance as the particle size decreases.

Equation 1 assumes a rigid spherical NP geometry. However, NPs used in experiments are usually surface ligated with a variety of nonrigid functionalizing molecules.¹⁴ Commonly, polymers¹⁵ or short organic molecules¹⁶ coat NP cores in the

* To whom correspondence should be addressed, steven.nielsen@utdallas.edu.

capacity of passivating layers, modifiers, or precursors.^{14,16} Incorporation of ligands changes the surface character of the NP and can modify the equilibrium position η_0 by changing γ_{pw} and γ_{po} . Ligands can also affect the desorption energy of a particle from the interface. Equation 1 predicts the free energy of localization scales as R^2 which gives energies of the same order as the thermal energy (k_BT) for small NPs. To prevent NP thermal desorption from the interface, some researchers use amphiphilic ligands which may impart additional stability. For example, tetra(ethylene glycol)dodecanethiol coated $R = 1$ nm gold NPs have been used to stabilize oil-in-water emulsions.¹⁷

Regardless of the type of ligand, the flexibility of these “soft” surface layers imparts a deformability to the NP which is increasingly important as the core radius and ligand length become comparable. The applicability of Young’s theory is less clear-cut for deformable nanoparticles, in particular the assumption of a fixed (effective) geometry of the NP.

We address this issue using molecular dynamics (MD) studies carried out on small deformable NPs at a representative oil/water interface. The sizes of the components are such that the core and the functionalizing layer are comparable. First we calculate the free energy profiles of coated NPs in the vicinity of an oil/water interface, and compare to Young’s theory. We show that assuming the equilibrium position is related to the balance of NP/solvent surface tensions can lead to erroneous results. Subsequently, we focus on the overall shape of the NP with an emphasis on its deformability. We discuss how this deformability is responsible for the error and propose a quantitative measure of NP deformation.

Methods

System Composition. To carry out the simulations, phase-separated oil/water simulation boxes each containing a surfactant functionalized NP were prepared as shown in Figure 1. Heptane is chosen as the oil phase and both water and heptane are represented through coarse grained (CG) models. The NP core is modeled as a rigid hydrophobic sphere of 5.6 Å radius. The di(ethylene glycol)dodecyl surfactants, which are also coarse grained, are tethered onto the core at their hydrophobic terminii following our previously published procedure.^{9,18} The potential for this tethering bond is taken as $U(r) = k(r - 8.6 \text{ \AA})^2$ where r is the distance of the tail bead from the center of the core and $k = 100 \text{ kcal mol}^{-1} \text{ \AA}^{-2}$ is the force constant of the bond. This potential tethers the tail of the surfactant 3.00 Å away from the surface of the core.¹⁸ This tethering potential allows for mobility of the surfactant over the NP core surface. The mobility can be rationalized in two ways: (1) some bonds such as the gold–thiol bond are genuinely mobile,¹⁹ or (2) diffusion results in an equilibrated system, which could occur through ligand adsorption/desorption for real systems.²⁰ Furthermore, studies we have carried out on systems with the surfactants chemisorbed to specific locations on the core show remarkably similar properties to the systems with mobile bonds (see Supporting Information). For more details of the force field we refer any interested readers to the primary references.^{18,21}

Four NP systems were chosen with 0, 20, 45, and 80 surfactants grafted onto the core to encompass the experimentally relevant surface densities. To put these values in context, if we assume a gold NP of the same radius, the number of adsorption sites available would be ≤ 49 .²² Images of these NPs can be seen in Figure 4.

Determining the Interfacial Free Energy Profiles of the NPs. The free energy profiles of the NPs in the vicinity of the oil/water interface are computed from constrained molecular

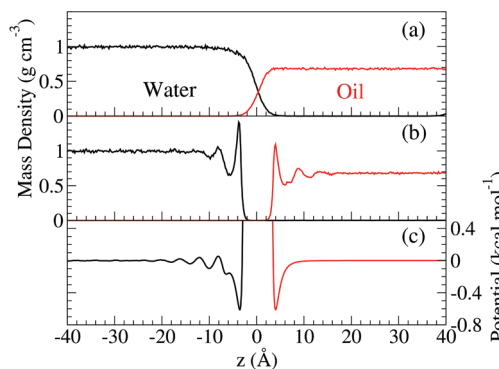


Figure 2. The top panel (a) shows the mass density profile of a water/heptane simulation box with no external potential applied. The middle panel (b) shows the density profile after application of the partitioning potential. The potentials applied on the oil and water phases are shown in the bottom (c) panel, where the water potential is engineered to attenuate density oscillations in the water phase.

dynamics (CMD) simulations of the different systems at fixed η values, from $\eta = -60 \text{ \AA}$ to $\eta = 60 \text{ \AA}$ at intervals of $\sim 2 \text{ \AA}$.

By choosing η as a progress variable and collecting the mean forces of constraint, we may use thermodynamic integration (TI) to obtain the free energy profiles for the NPs as a function of η . However, meniscus formation in regions B and D (see Figure 3) resulted in hysteresis in the computed free energy profiles. To overcome this problem, separate free energy simulations were carried out to unambiguously determine the oil to water transfer free energy $\Delta G_{o \rightarrow w}$ as described below. The formation of the meniscus occurred predominantly in region D; hence the free energy curves in this region were adjusted so as to yield the correct transfer free energies. These modified free energy profiles are given in Figure 4. At each value of η , the modified profiles correctly average over all interface fluctuations except for the large meniscus formation in region D. Here hysteresis makes inaccessible the relative weight to assign to the meniscus-formed and meniscus-broken interface configurations.

Measurement of the NP Transfer Free Energy. The free energy profiles of the NPs as a function of their interfacial position η were obtained using constrained MD followed by thermodynamic integration (TI). However, meniscus formation led to an observed hysteresis in the profile, resulting in uncertainty in the transfer free energy values $\Delta G_{o \rightarrow w}$. Since the transfer free energy is a state function, we changed the path for its calculation to avoid hysteresis.

To eliminate hysteresis, the oil/water interface was rigidified through the use of wall potentials to which the NP is transparent. The wall potentials are based on a weakly attractive Lennard-Jones potential centered at $z = 0$, such that the solvents are separated by the wall but still feel an attractive potential which prevents them from diffusing away from the interface. Mass density profiles of oil and water before application of the dividing potential (Figure 2a) and after the application of the dividing potential (Figure 2b) are shown in Figure 2. The NPs (including the surfactant ligands) do not directly feel the effects of this potential. Since the introduction of a rigid wall tends to structure the fluid adjacent to it, we iteratively adjusted the potential to attenuate water structuring. The potential shown in Figure 2c eliminates almost all of the water structuring that would be caused by a purely Lennard-Jones function. The intramolecular interactions in heptane make it less susceptible to structuring so that we simply used a Lennard-Jones function for the heptane wall. After application of this potential wall, the TI method can be accurately used because a meniscus does

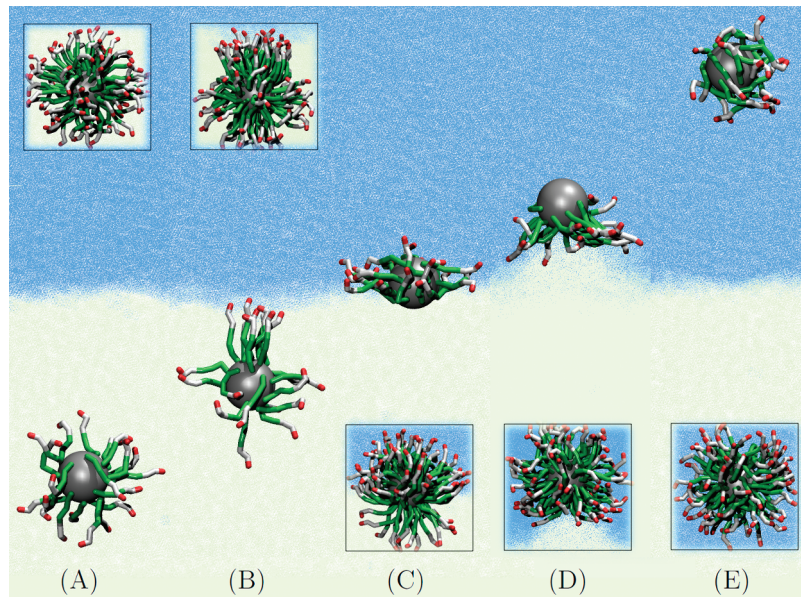


Figure 3. Constrained molecular dynamics simulations were carried out on the NPs at $\sim 2 \text{ \AA}$ intervals from deep in heptane (A) to deep in water (E). Four nanoparticle systems were used with 0, 20, 45, and 80 surfactants tethered to the NP core, respectively. Snapshots of the 20 surfactant system are shown in the main figure while the insets show the 80 surfactant system at similar positions.

not form. The resulting free energy profile is influenced by the artificial wall constraint imposed on the interface. In particular, this indirectly affects the constraint force on the NP. However, the transfer free energy $\Delta G_{\text{o} \rightarrow \text{w}}$ is unaffected by this artificial transfer path.

Antistructuring Water Wall Potential. The structuring of water at a rigid wall is well-known.^{23–25} This structuring extends deep into the water phase and would cause oscillations in the free energy profiles calculated in determining the transfer free energy. In principle these oscillations would not affect the $\Delta G_{\text{o} \rightarrow \text{w}}$ value as long as the η -range used extends far enough. However, to alleviate this structuring and hence use a smaller η -range the potential applied on the water beads is adjusted to oppose the structuring. The adjustment is made iteratively according to the correction function²⁶

$$U_{n+1}(z) = U_n(z) + k_B T \ln \left[\frac{g_n(z)}{g_{\text{target}}(z)} \right] \quad (3)$$

where $U_n(z)$ is the n th iteration of the potential, k_B the Boltzmann constant, and T the temperature. Here, $g_n(z)$ is the volume number density of water beads for the n th iteration and $g_{\text{target}}(z)$ is the target density profile. We chose a horizontal target density profile beyond the first hydration layer. Starting from a simple Lennard-Jones potential, two iterations of this scheme produced the potential plotted in Figure 2 which gives very little structuring of water beyond the above-mentioned primary hydration layer.

Simulation Details. Molecular dynamics simulations were carried out with the MPDYN²⁷ package using the force field of Shinoda et al²¹ and Kalescky et al.¹⁸ The rRESPA²⁸ multiscale time step algorithm was used with a time step of 10 fs for all long ranged intermolecular interactions and a 1 fs time step for all other interactions. The simulation box sizes for the CMD runs were $\approx 130 \times 130 \times 260 \text{ \AA}^3$ corresponding to ≈ 50000 CG beads. The Nosé-Hoover thermostat,²⁹ at 300.15 K and an Andersen barostat³⁰ (acting parallel to \hat{n} with an external pressure of 0.1 MPa) were applied for all simulations. All

simulations were initially run for 1 ns prior to data collection runs of at least 5 ns.

Results and Discussion

Representative snapshots of the system are shown in Figure 3. From our observations, five distinct regions can be identified with regard to the behavior of the ligands. The regions are (A) deep in the oil phase, (B) in the oil phase close to the interface, (C) at the interface, (D) in the water phase close to the interface, and (E) deep in the water phase.

Free Energy Profiles. The free energy profiles (see Figure 4) illustrate the interfacial activity of all the NP systems. On the basis of the transfer free energies, the presence of 20 surfactants increases the hydrophobicity of the NP surface when compared to the bare NP. This is because the alkane block of the surfactants is exposed to the solvent. With higher coverage of surfactants (45, 80) the alkane segments of the surfactants are buried by the head groups, creating a hydrophilic surface which results in successively lower $\Delta G_{\text{o} \rightarrow \text{w}}$ values. The profiles are also broader than those predicted by theory because of interactions between the surfactants and the interface at distances greater than contact due to dispersion forces.

It is apparent that addition of surfactants onto the core successively stabilizes the interfacial localization. To reconcile this result with the theory given in eq 1, we must increase the effective radius of the NP. In doing so we assume that the theory captures the NP behavior by assigning an effective radius (R_{eff}) to the particle, whereby the behavior of the whole NP is captured in an implicit manner. An expression for this effective radius can be derived using the transfer free energy, $\Delta G_{\text{o} \rightarrow \text{w}} = 4\pi R^2(\gamma_{\text{pw}} - \gamma_{\text{po}})$, in conjunction with Young's equation (eq 2)

$$R_{\text{eff}} = -\frac{\Delta G_{\text{o} \rightarrow \text{w}}}{4\pi\eta_0\gamma_{\text{ow}}} \quad (4)$$

This simple expression is appealing because it does not involve NP/solvent surface tensions, which are difficult to determine (either by experimental or theoretical means) but

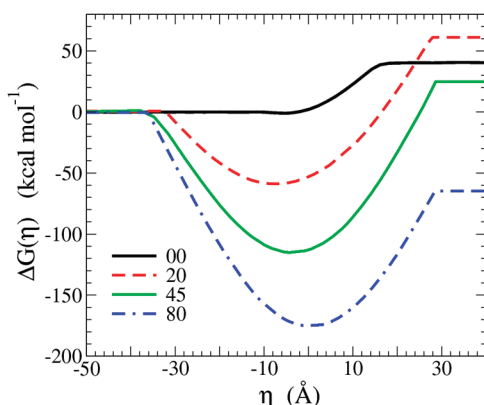


Figure 4. The free energy profiles of the four NP systems. All the NPs show surface activity, which is augmented with surfactant functionalization. The equilibrium positions (η_0 , in Å), free energy minima ($\Delta G(\eta_0)$, in kcal mol⁻¹), oil to water transfer free energies ($\Delta G_{o \rightarrow w}$, in kcal mol⁻¹) and the effective radii (R_{eff} , in Å) from eq 4 are given to the right. Details on how accurate values for η_0 are obtained may be found in the Supporting Information.

rather only terms which are accurately known, namely, η_0 , $\Delta G_{o \rightarrow w}$ and γ_{ow} (50.1 mN m⁻¹). The resulting R_{eff} values for the four NP systems are given in Figure 4. It is apparent that these results are erroneous as some of the values (for the 45 and 80 surfactant coated NPs) are not physical.

To explain this unphysical result, we focus on the interpretation of the NP equilibrium position η_0 . Young's theory equates η_0/R to the relative surface tensions of the two NP/solvent interfaces. Consequently, a rigid spherical NP with $\eta_0 = 0$ should have equal surface tensions with the two solvents and thus $\Delta G_{o \rightarrow w} = 0$. The free energy profile for the 80 surfactant system clearly shows that this is not the case: $\eta_0 \approx 0$ but $\Delta G_{o \rightarrow w}$ is -64.8 kcal mol⁻¹. The asymmetry of the ligands between the two fluid phases can cause an unequal surface area of the NP in the two fluid phases. Therefore the surface tensions need not be similar between the NP and the two fluid environments to observe $\eta_0 \approx 0$. The converse is also true, namely, $\Delta G_{o \rightarrow w} = 0$ need not correspond to $\eta_0 = 0$. These inconsistencies have important implications because η_0/R (equivalently the equilibrium contact angle) is typically how the localization behavior is assessed experimentally. It is clear for the systems considered here that interpreting contact angles in the framework of Young's theory leads to an incorrect understanding of the energetics of NP localization at a fluid/fluid interface. Moreover, incorporation of line tension into Young's theory does not change this conclusion as demonstrated in detail in the Appendix.

Shape Deformation. We have argued that shape changes of the NP can alter the interpretation of contact angle data. Previous work by Bresme and co-workers³¹ has established that alkanethiol passivated NPs show "lenslike" shapes at an air/water interface. This could be expected from an energetics standpoint whereby adopting a disklike shape removes more fluid/fluid contact. In other publications the same authors derive the theoretical free energy expression for anisotropic rigid particles at a liquid/liquid interface, which predicts deeper free energy wells for oblate spheroids³² compared to their spherical counterparts. In bulk phases however, the flexibility of the functionalizing molecules allows the NPs to adopt a spherical shape. Discussion of the energetics of particle adsorption is rarely inclusive of the concept of shape deformation. As a first step in motivating this discussion, we study the ability of a NP to deform in response to its environment.

To illustrate the NP deformability two measures of surfactant conformation are used. First, the radius of gyration of the three

	η_0	$\Delta G(\eta_0)$	$\Delta G_{o \rightarrow w}$	R_{eff}
Bare	-5.34	-1.0	40.4	8.36
20 Surfactants	-7.31	-59.4	61.1	9.23
45 Surfactants	-3.69	-116.6	25.0	7.49
80 Surfactants	0.45	-174.9	-64.8	159.15

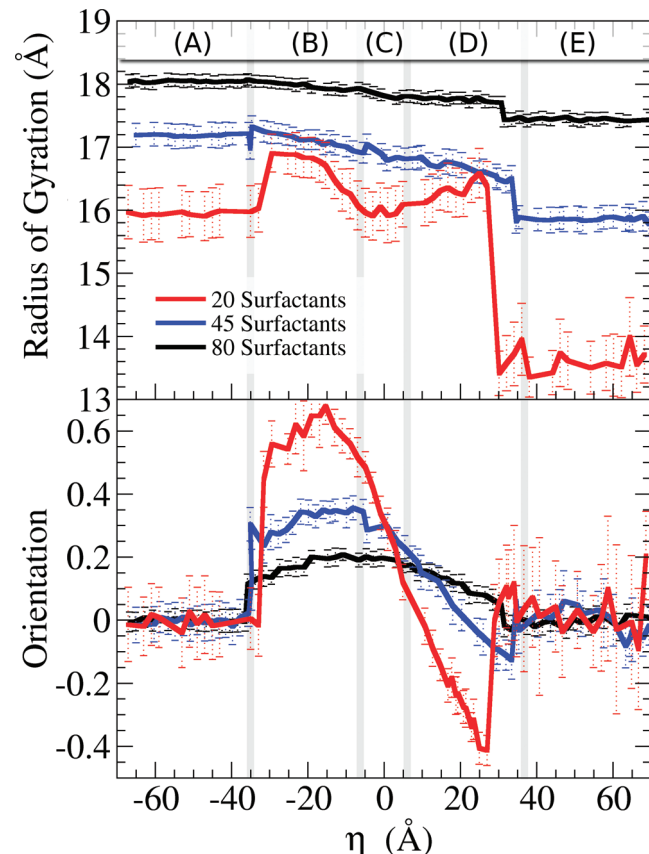


Figure 5. The top panel shows the radius of gyration R_g for the three functionalized NP systems as a function of η . The bottom panel shows a measure of the orientation of the surfactants, given by the averaged dot product of \mathbf{h} and $\hat{\mathbf{n}}$ as a function of η for the same systems.

coated NPs is plotted in Figure 5 as a function of η . The radius of gyration R_g was chosen as a well-defined measure of the extension of the ligands which also incorporates the particle core size. Here

$$R_g^2 = \frac{1}{N} \left\langle \sum_{i=1}^N (r_i - r_{\text{NP}})^2 \right\rangle \quad (5)$$

where r_i is the position of the i th surfactant bead, r_{NP} is the nanoparticle core position, and N the total number of surfactant

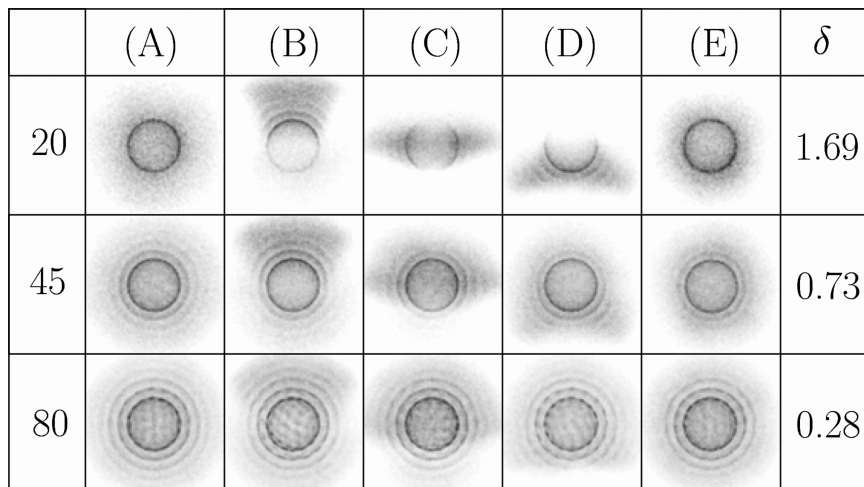


Figure 6. Average bead density projected onto a plane parallel to the interface normal $\hat{\mathbf{n}}$. The letter denotes the region while the number denotes the surfactant coverage of the NP core. As the NP moves across the interface, the surfactants show preferential orientations. The deformability values (δ) explained in the text are given in the rightmost column.

beads. To characterize the surfactant orientation, a second measure given by

$$\left\langle \sum_{i=1}^S \hat{\mathbf{n}} \cdot (\vec{h}_i / |\vec{h}_i|) / S \right\rangle \quad (6)$$

was used (see Figure 5), which evaluates the averaged dot product of \vec{h} (the NP center to surfactant head vector) and $\hat{\mathbf{n}}$ (the interface normal unit vector) as a function of η . Here S is the number of surfactants bound to the NP.

From these two measures it is clear that in the uniform hydrophobic environment of region A, the ligands are swollen but show no preferred orientation. In region B, the surfactant ligands extend upward to interact with the interface. At the interface (region C) the ligands form an annular ring around the NP core which curves up into the water phase. The behavior of the NP in regions D and E is similar to that in regions B and A, respectively, except that in water the ligands tend to collapse onto the NP core leading to a smaller radius of gyration. It is clear from these measures that the NP functionalized with 80 surfactants shows the least variation in its properties while the greatest variation is shown by the 20 surfactant coated NP. In other words the 20 surfactant system is “softer” than the 80 surfactant system.

The softness of a particle is a concept acknowledged in many fields. For example, measures of softness are often used to predict packing patterns of NP superstructures.³³ One measure of softness is the ratio of the NP core radius to the fully extended length of the surface ligand.^{33,34} Such a measure would be inadequate for our purposes because, for example, the softness value would not change with bound surfactant density. Here we propose a simple measure to quantify this effect: the system deformability

$$\delta = \frac{C|R_g(o) - R_g(w)|}{R_g(w) + R_g(o)} \quad (7)$$

where $R_g(w)$ and $R_g(o)$ are the radius of gyration of the NP in bulk water and bulk oil, respectively, and C is a scaling factor taken to be $C = 20$. The susceptibility to deform is measured through the difference of R_g values in the bulk solvents, since

the ligands will swell to different degrees in response to their hydrophobic/hydrophilic environment. Measurement of R_g in a homogeneous environment also avoids the need to quantify nonspherical geometries.

The δ values for the surfactant functionalized systems are given in Figure 6, which also shows the ligand density around the three coated NP systems in the same regions (A–E) shown in Figure 3. It can be noted that systems with high deformability show large variations in their properties (see Figure 5) while systems with low deformability show little variation.

Conclusions

In summary we have used molecular dynamics simulations to characterize the behavior of surface-ligated NPs in the vicinity of an oil/water interface. Studies of four NPs with different coverages of a surfactant ligand showed that the coating has a large effect on the NP interfacial activity. Inadequacies in Young’s equation were exposed due to the assumption that the contact angle represents the difference in NP/solvent surface tensions. Moreover, it is not apparent that modifications of Young’s equation aid in improving our physical understanding of the observed behavior. For example, addition of a free energy contribution due to line tension still results in $\Delta G_{o-w} = 0 \leftrightarrow \eta_0 = 0$, which was the same problem we found with Young’s equation. The main source of error in the theory is brought about by the flexibility of the surface functionalizing ligands which allow the particle to deform from an idealized spherical shape. Furthermore, the change in the NP interface binding free energy and transfer free energy with the number of bound surfactants is significant enough that a proper theoretical treatment may need to explicitly account for the deformable ligand surface. We defined a system deformability parameter δ to quantify the susceptibility of different NPs to deform. This measure may prove useful in studies which explicitly include ligands in the discussion of the physical behavior of NPs in the vicinity of a fluid interface.

Appendix

Proof that $\eta_0 = 0 \leftrightarrow \Delta G_{o-w} = 0$ in the Presence of Line Tension τ . It is clear from eq 2 and the definition of $\Delta G_{o-w} = 4\pi R^2(\gamma_{pw} - \gamma_{po})$ that $\eta_0 = 0 \leftrightarrow \Delta G_{o-w} = 0$ for Young’s theory. However for a deformable NP we showed this is not true. Here

we prove that supplementing Young's equation with a contribution due to line tension does nothing to resolve this discrepancy.

According to the modified Young's equation³⁵ the free energy of a radius R particle at a distance η from an oil/water interface, from a reference state in oil ($\eta = -R$), is

$$\Delta G(\eta) = 2\pi R^2(1 + \eta/R)(\gamma_{\text{pw}} - \gamma_{\text{po}}) - \gamma_{\text{ow}}\pi(R^2 - \eta^2) + 2\pi\tau\sqrt{R^2 - \eta^2} \quad (8)$$

Here τ is the three-phase line tension and $2\pi(R^2 - \eta^2)^{1/2}$ is the length of the three-phase contact line.

The derivative of eq 8 with respect to η is

$$\frac{\partial \Delta G}{\partial \eta} = 2\pi R(\gamma_{\text{pw}} - \gamma_{\text{po}}) + 2\pi\gamma_{\text{ow}}\eta - 2\pi\tau\eta(R^2 - \eta^2)^{-1/2} \quad (9)$$

We would like to prove that $\eta_0 = 0 \Leftrightarrow \Delta G_{\text{o} \rightarrow \text{w}} = 0$, where η_0 is the equilibrium position of the particle and $\Delta G_{\text{o} \rightarrow \text{w}}$ is the oil to water transfer free energy.

Proof that $\eta_0 = 0 \Rightarrow \Delta G_{\text{o} \rightarrow \text{w}} = 0$. Since η_0 corresponds to a free energy minimum, the left-hand side of eq 9 is zero. Therefore

$$0 = 2\pi R(\gamma_{\text{pw}} - \gamma_{\text{po}}) \Rightarrow \gamma_{\text{pw}} = \gamma_{\text{po}}$$

Since $\Delta G_{\text{o} \rightarrow \text{w}} = 4\pi R^2(\gamma_{\text{pw}} - \gamma_{\text{po}})$, it follows that $\Delta G_{\text{o} \rightarrow \text{w}} = 0$; i.e., the transfer free energy is zero when the particle has an equilibrium position (free energy minimum) of $\eta_0 = 0$.

Proof That $\Delta G_{\text{o} \rightarrow \text{w}} = 0 \Rightarrow \eta_0 = 0$. When the transfer free energy is zero, the first term on the right-hand side of eq 9 is zero. We can find the equilibrium position, η_0 , by finding the global minimum of $\Delta G(\eta)$ with respect to η (eq 8). First let us find the extremum points by setting $\partial \Delta G / \partial \eta = 0$ in eq 9

$$0 = 2\pi\gamma_{\text{ow}}\eta_0 - 2\pi\tau\eta_0(R^2 - \eta_0^2)^{-1/2} \quad (10)$$

Clearly $\eta_0 = 0$ is a solution. By substituting $\eta_0 = 0$ into eq 8, with $\Delta G_{\text{o} \rightarrow \text{w}} = 0$, we obtain

$$\Delta G(0) = -\gamma_{\text{ow}}\pi R^2 + 2\pi\tau R$$

The free energy expression when the particle is completely submerged in either bulk phase corresponds to $\Delta G = 0$ (because $\gamma_{\text{pw}} = \gamma_{\text{po}}$). Therefore, as long as $\gamma_{\text{ow}} \geq 2\tau/R$, $\eta_0 = 0$ gives a lower free energy than when $\eta = -R$ or R . For a representative particle size of $R = 1$ nm at an oil/water interface with $\gamma_{\text{ow}} \sim 50$ mN m⁻¹, this corresponds to a threshold value of $\tau \sim 2.5 \times 10^{-11}$ N. Specifically, with a negative line tension or a positive line tension lower than 2.5×10^{-11} N, the particle will have lower energy at $\eta = 0$ compared to the bulk liquid phases.

Since $\eta_0 = 0$ is only one solution to eq 10, to look for other possible solutions consider $\eta_0 \neq 0$. In this case, rearrangement of eq 10 gives

$$\gamma_{\text{ow}} = \tau(R^2 - \eta_0^2)^{-1/2}$$

This equation only holds when $\tau \geq 0$, since both γ_{ow} and $(R^2 - \eta_0^2) \geq 0$. For $\tau \geq 0$, we can simplify this equation to obtain

$$\eta_0^2 = R^2 - \frac{\tau^2}{\gamma_{\text{ow}}^2} \quad (11)$$

To see if this η_0 value corresponds to a global minimum, we again substitute it into the free energy expression (eq 8)

$$\begin{aligned} \Delta G(\eta_0) &= -\gamma_{\text{ow}}\pi R^2 - (R^2 - \tau^2/\gamma_{\text{ow}}^2) + \\ &\quad 2\pi\tau\sqrt{R^2 - (R^2 - \tau^2/\gamma_{\text{ow}}^2)} \\ \Rightarrow \Delta G(\eta_0) &= -\frac{\pi\tau^2}{\gamma_{\text{ow}}} + 2\frac{\pi\tau^2}{\gamma_{\text{ow}}} = \frac{\pi\tau^2}{\gamma_{\text{ow}}} \end{aligned}$$

Clearly this η_0 value corresponds to a free energy which is necessarily higher than when the particle is completely submerged in either liquid.

Therefore for a particle with zero transfer free energy, either the equilibrium position will be at $\eta_0 = 0$ or the particle is so destabilized by the line tension that it will show only metastable states at the interface.

Supporting Information Available: Details on the method of evaluating η_0 and comparison of mobile surfactants versus statically bound surfactants for the 20 surfactant system. This material is available free of charge via the Internet at <http://pubs.acs.org>.

References and Notes

- (1) *Colloids and Colloid Assemblies*; Caruso, F., Ed.; Wiley-VCH: Weinheim, 2004.
- (2) Kinge, S.; Creg-Calama, M.; Reinhoudt, D. N. *ChemPhysChem* **2008**, *9*, 20–42.
- (3) Zhang, H.; Edwards, E. W.; Wang, D.; Mohwald, H. *Phys. Chem. Chem. Phys.* **2006**, *8*, 3288–3299.
- (4) Boker, A.; He, J.; Emrick, T.; Russell, T. P. *Soft Matter* **2007**, *3*, 1231–1248.
- (5) Bresme, F.; Oettel, M. *J. Phys.: Condens. Matter* **2007**, *19*, 413101–413133.
- (6) Chen, X. Y.; Li, J. R.; Jiang, L. *Nanotechnology* **2000**, *11*, 108–111.
- (7) Santhanam, V.; Liu, J.; Agarwal, R.; Andres, R. P. *Langmuir* **2003**, *18*, 7881–7887.
- (8) Pieranski, P. *Phys. Rev. Lett.* **1980**, *45*, 569–572.
- (9) Although the terminal ligand bead is modeled using hydrocarbon parameters, it should be conceived as a moiety which is chemisorbed to the NP core.
- (10) Amirfazli, A.; Neumann, A. W. *Adv. Colloid Interface Sci.* **2004**, *110*, 121–141.
- (11) Aveyard, R.; Clint, J. H. *J. Chem. Soc., Faraday Trans.* **1996**, *92*, 85–89.
- (12) Huang, D. M.; Geissler, P. L.; Chandler, D. *J. Phys. Chem. B* **2001**, *105*, 6704–6709.
- (13) Cheung, D. L.; Bon, S. A. F. *Phys. Rev. Lett.* **2009**, *102*, 066103.
- (14) Sperling, R. A.; Parak, W. J. *Philos. Trans. R. Soc. London, Ser. A* **2010**, *368*, 1333–1383.
- (15) Grubbs, R. B. *Polym. Rev.* **2007**, *47*, 197–215.
- (16) Neuouze, M.-A.; Schubert, U. *Monatsh. Chem.* **2008**, *139*, 183–195.
- (17) Glogowski, E.; Tangirala, R.; He, J.; Russell, T. P.; Emrick, T. *Nano Lett.* **2007**, *7*, 389–393.
- (18) Kalesky, R. J. B.; Shinoda, W.; Moore, P. B.; Nielsen, S. O. *Langmuir* **2009**, *25*, 1352–1359.
- (19) Vericat, C.; Vela, M. E.; Salvarezza, R. C. *Phys. Chem. Chem. Phys.* **2005**, *7*, 3258–3268.
- (20) Hostetler, M. J.; Templeton, A. C.; Murray, R. W. *Langmuir* **1999**, *15*, 3782–3789.
- (21) Shinoda, W.; DeVane, R.; Klein, M. L. *Soft Matter* **2008**, *4*, 2454–2462.
- (22) The number of atoms in a crystalline solid may be approximated using the formula $R = r_s N^{1/3}$ where R is the particle radius, N is the number of atoms in the particle, and r_s is the Wigner–Seitz radius. See, for example: Zheng, J.; Nicovich, P. R.; Dickson, R. M. Highly Fluorescent

- Noble-Metal Quantum Dots. *Annu. Rev. Phys. Chem.* **1980**, *58*, 409–431. Taking $r_s = 1.5875 \text{ \AA}$, the number of atoms for a radius 5.6 Å gold particle is ~49.
- (23) Israelachvili, J. N. *Intermolecular and Surface Forces*; Academic Press: New York, 1985.
- (24) Xu, D.; Leng, Y.; Chen, Y.; Li, D. *Appl. Phys. Lett.* **2009**, *94*, 201901.
- (25) Xue, L.; Kebinski, P.; Phillipot, S. R.; Choi, S. U. S.; Eastman, J. A. *Int. J. Heat Mass Transfer* **2004**, *47*, 4277–4284.
- (26) Muller-Plathe, F. *ChemPhysChem* **2002**, *3*, 754–769.
- (27) Shinoda, W.; Mikami, M. *J. Comput. Chem.* **2003**, *24*, 920–930.
- (28) Tuckerman, M. E.; Berne, B. J.; Martyna, G. J. *J. Chem. Phys.* **1991**, *94*, 6811–6815.
- (29) Hoover, W. G. *Phys. Rev. A* **1985**, *31*, 1695–1697.
- (30) Andersen, H. C. *J. Chem. Phys.* **1980**, *72*, 2384–2393.
- (31) Tay, K. A.; Bresme, F. *J. Am. Chem. Soc.* **2006**, *128*, 14166–14175.
- (32) Faraudo, J.; Bresme, F. *J. Chem. Phys.* **2003**, *118*, 6518–6528.
- (33) Whetten, R. L.; Shafiqullin, M. N.; Khouri, J. T.; Schaaf, T. G.; Verzmar, I.; Wilkinson, A. *Acc. Chem. Res.* **1999**, *32*, 397–406.
- (34) Landman, U.; Luedtke, W. D. *Faraday Discuss.* **2003**, *125*, 1–22.
- (35) Wang, J. Y.; Betelu, S.; Law, B. M. *Phys. Rev. E* **2001**, *63*, 031601.

JP105355Y